Journal of Materials Chemistry B

Surface Plasmon-Photosensitizer Resonance Coupling: An Enhanced Singlet Oxygen Production Platform for Broad-Spectrum Photodynamic Inactivation of Bacteria

Journal:	*Journal of Materials Chemistry B*
Manuscript ID:	TB-ART-07-2014-001139.R1
Article Type:	Paper
Date Submitted by the Author:	07-Aug-2014

Complete List of Authors:	Hu, Bo; University of Cincinnati, Department of Chemistry Cao, Xian; University of Cincinnati, Chemistry Nahan, Keaton; University of Cincinnati, Chemistry Caruso, Joseph; University of Cincinnati, Chemistry Tang, Hong; University of Cincinnati, Drug Discovery Center Zhang, Peng; University of Cincinnati, Chemistry

RSCPublishing

ARTICLE

Surface Plasmon-Photosensitizer Resonance Coupling: An Enhanced Singlet Oxygen Production Platform for Broad-Spectrum Photodynamic Inactivation of Bacteria

Cite this: DOI: 10.1039/x0xx00000x

Received ooth January 2014,
Accepted ooth January 2014

DOI: 10.1039/x0xx00000x

www.rsc.org/

Bo Hu,[a] Xian Cao,[a] Keaton Nahan,[a] Joseph Caruso,[a] Hong Tang,[b]* Peng Zhang [a]*

Singlet oxygen plays a critical role in a great number of applications including photodynamic therapy of cancers, photodynamic inactivation of microorganisms, photooxidation, and photodegradation of polymers. Herein we demonstrate a general platform to improve singlet oxygen production via resonance coupling between surface plasmon and photosensitizers. By loading photosensitizers into mesoporous silica containing silver nanoparticles, strong resonance coupling between the photosensitizers and silver core markedly increases the singlet oxygen production, by up to three orders of magnitude in some cases. It is observed that the more spectral overlap between the surface plasmon resonance spectrum of silver core and the photosensitizers' absorption spectra, the greater the singlet oxygen production. As-synthesized hybrids have shown exceptionally high photoinactivation efficiency against both Gram-positive and Gram-negative bacteria. This work establishes a general platform to improve singlet oxygen production and to develop more effective and efficient hybrid photosensitizers for broad-spectrum photodynamic inactivation of bacteria.

Introduction

The ground electronic state of molecular oxygen, $O_2(^3\sum_g^-)$, is a spin triplet.[1, 2] The two electronically excited singlet states are $O_2(^1\Delta_g)$ and $O_2(^1\sum_g^+)$, at 94 and 157 KJ mol^{-1} above the ground state, respectively.[3] The $O_2(^1\sum_g^+)$ state has a rather short lifetime, due to the spin-allowed transition to the $O_2(^1\Delta_g)$ state. The $O_2(^1\Delta_g)$ state has a relatively long lifetime, 10^{-6}-10^{-3} s in solution, because of the spin-forbidden transition to $O_2(^3\sum_g^-)$, and can be observed experimentally in the absorption and emission at ~1270 nm.[4] The $O_2(^1\Delta_g)$ receives a lot of attention and is commonly referred to as "singlet oxygen".

The most convenient method of singlet oxygen production is the photosensitization of sensitizers in the presence of light and oxygen.[1,4,5] Photosensitized production of singlet oxygen plays a central role in many applications, such as photodynamic therapy of cancers, photodynamic inactivation of microorganisms, photoinduced oxidation, photodegradation of polymers, wastewater treatment, and fine chemical synthesis.[4,6-9] Great progresses have been made in identifying, designing and synthesizing molecules as efficient photosensitizers.[4] Even noble metal nanostructures themselves have demonstrated the capability of singlet oxygen production.[10,11] Still, the ability of noble metal nanostructures to enhance the production of singlet oxygen remains largely unexploited.[12-22]

Plasmon-molecular resonance coupling, where light-absorbing molecules near metal nanoparticles exhibit strong absorption due to the localized surface plasmon, has emerged as a new modality in the development of photonic devices and optically responsive and active nanocomplexes.[23-25] The coupling usually leads to the hybridization of the plasmon and molecular resonance, forming hybrid states with spectral characteristics distinct from those of the individual constituents. The plasmon-molecular resonance coupling strength is highly sensitive to the spectral overlap between the molecular absorption and the surface plasmon of metal nanostructures. For instance, it has been shown that the coherent resonance coupling between the exciton of J-aggregate molecule and the surface plasmon of metal nanoparticles is constructive for Ag nanoparticles (AgNPs) leading to a long-lived exciton, while destructive for Au nanoparticles with a reduced exciton lifetime by two orders of magnitude.[26] Another interesting observation is that resonance coupling can lead to the unconventional energy transfer from metal nanoparticles to light-absorbing molecules.[27,28] Metal-molecule hybrid structures have also been proposed theoretically to enhance photochemical production in the photosynthetic system.[29]

Photodynamic inactivation (PDI) of bacteria has become an emerging and evolving strategy against infectious diseases, especially those related to multidrug resistance, because microorganism does not appear to readily develop resistance toward PDI. Multidrug-resistant bacterial strains are shown to be killed by PDI as easily as their native counterparts.[30-34] When the level of produced reactive oxygen species (ROS) exceeds bacterial detoxification and repair capabilities, ROS can damage intracellular DNA, RNA, proteins, lipids, and cytoplasmic membrane, leading to bacterial death.[30,35] It is accepted that Gram-positive bacteria can easily take up most neutral or anionic photosensitizers and be readily photoinactivated, while it is not the case for Gram-negative bacteria because of their different outer membrane structures.[30,34] The difference in membrane permeability between Gram-positive and

Gram-negative bacteria has led the development of photosensitizers toward polycationic conjugates or cationic moieties to facilitate their uptake by the bacterial cells.[36-41] On the other hand, some studies have shown that singlet oxygen, when produced close to bacteria in sufficient abundance, can diffuse into the bacterial cells causing fatal damage to the cells.[30,42] Accordingly, photosensitizers with good singlet oxygen production efficiency will be highly desired, regardless of their charge properties.[43]

Herein we report a general singlet oxygen production platform based on the surface plasmon-photosensitizer resonance coupling between AgNPs and photosensitizers. Strong surface plasmon-photosensitizer resonance coupling significantly increases the singlet oxygen production by up to three orders of magnification. We systematically studied the PDI activity of the hybrid photosensitizer on model Gram-positive bacterium, *Staphylococcus epidermidis*, and Gram-negative bacteria, *Escherichia coli* and drug-resistant *Acinetobacter baumannii*. The AgNP-photosensitizer hybrids can photodynamically inactivate all three bacteria without pre-incubation and with highly enhanced efficiency as compared to the pure photosensitizer molecule and AgNPs.

Experimental

Chemicals and Materials. Cetyltrimethylammonium bromide (CTAB), formaldehyde solution (37 %), ammonium nitrate, sodium hydroxide, nitic acid (68%), and sodium cyanide, were purchased from Thermo Fisher. Dimethylformamide (DMF), tetraethyl orthosilicate (TEOS), absolute anhydrous ethanol, silver nitrate, tris(2,2'-bipyridyl)dichlororuthenium(II) hexahydrate (RuBPy), and rose bengal (RB), were from Sigma Aldrich. Hematoporphyrin IX dihydrochloride (HPIX), Meso-tetra(4-carboxyphenyl) porphine (TCPP), Cu(II) meso-tetra(4-carboxyphenyl) porphine (Cu-TCPP), and meso-porphyrin IX (PIX) were from Frontier Scientific. All chemicals were used without additional purification. PBS buffer came from Nalgene. *S. epidermidis* (ATCC 35984), *E. coli* (ATCC 35218), and *A. baumannii* (ATCC 19606) were from ATCC.

Synthesis of Ag@mSiO$_2$ nanoparticles. Silver-mesoporous silica core-shell nanoparticles (Ag@mSiO$_2$) were synthesized by a facile method using silver nitrate as the precursor, formaldehyde as the reducing agent, CTAB as the stabilizer and template, TEOS as the silica source, and sodium hydroxide as the catalyst.[44] In a typical run, 0.02 g of CTAB was dissolved in a solution containing 9.8 mL of water and 0.24 mL of 0.5 M NaOH. After stirring at 80 ^{o}C for 10 min, 0.06 mL of 1.0 M formaldehyde solution and 0.24 mL of 0.1 M silver nitrate aqueous solution were added. Then 0.07 mL TEOS was added at a rate of 3 mL/h under stirring. After reaction at 80 ^{o}C under stirring for 2 h, the products were centrifuged and washed by ethanol. The surfactant template was removed by extraction in ethanol solution containing ammonium nitrate (6 g/L) at 50 ^{o}C for 30 min.

Synthesis of Ag@mSiO$_2$@photosensitizer hybrids. The freshly synthesized Ag@mSiO$_2$ nanoparticles were dispersed in 10 mL aqueous solution under stirring. Then, 10 mL DMF solution of respective photosensitizer (1 mM) was added and stirred at room temperature for 72 h. The products were centrifuged and washed by water and DMF three times to remove any unbound photosensitizers. Finally, the as-synthesized Ag@mSiO$_2$@photosensitizer hybrids were dispersed into 10 mL aqueous solution under sonication, and used as stock solutions.

Silver ion release measurements. Ag@mSiO$_2$ nanoparticle dispersion (~ 1.1 mg/mL) was prepared in diluted HNO_3 solution (pH 4.0), which can accelerate the oxidation of AgNPs under the ambient conditions and the release of Ag^+ into solution. The solution was exposed to air for 5 days, one sample collected each day. The released Ag^+ concentration of each sample was measured by a triple quadruple ICP-MS (ICP-QQQ, Agilent Technologies).

Fluorescence and phosphorescence measurements. A QM-40 spectrofluorometer (PTI Inc.) equipped with a high performance InGaAs photodiode and a lock-in amplifier (MODEL 410 single phase, Scitec Instruments Ltd.) was used to measure the fluoresence and phosphorescence spectra and lifetimes. Detection of the singlet oxygen production was carried out by monitoring its phosphorescence emission at ~1270 nm. The light source was a Xenon arc lamp, whose output passed through an optical chopper operating at a fixed frequency. Samples were loaded into a quartz cuvette and placed in a light-tight chamber, with the emission signal collected orthogonal to the excitation beam. An additional long-pass filter (850 nm cut-off) was used to remove any possible higher-order artifact signals. Samples were dispersed in DI water for testing. To remove the silver core out of Ag@mSiO$_2$@photosensitizer hybrids, excess amount of sodium cyanide (0.1 M) was added, which itself would not affect the photosensitizers adsorbed into the mesoporous silica.[45] All fluorescence, phosphorescence, and lifetime measurements of Ag@mSiO$_2$@photosensitizer hybrids were carried out on the same instrument. All photosensitizers were dissolved in PBS buffer solution (pH 7.4) before spectral measurement. The excitation wavelengths for fluorescence and singlet oxygen production are 403 nm, 400 nm, 400 nm, 393 nm, 460 nm, and 550 nm for HPIX, TCPP, Cu-TCPP, PIX, RuBPy, and RB, respectively. The emission bands center at 620 nm, 650 nm, 650 nm, 617 nm, 615 nm, and 576 nm, for HPIX, TCPP, Cu-TCPP, PIX, RuBPy, and RB, respectively.

PDI assays. Typically, overnight cultures of *S. epidermidis* (ATCC 35984), *E. coli* (ATCC 35218), and *A. baumannii* (ATCC 19606) were inoculated into PBS buffer solution (pH=7.4) and mixed with a series of concentrations of Ag@mSiO$_2$@HPIX hybrid, HPIX (dissolved in the same PBS buffer solution), or Ag@mSiO$_2$ nanoparticles. All bacterial suspensions (200 μL), including non-treated bacterial controls, were then placed in the wells of 96-well plates. The final cell concentration of the suspensions was ~10^6-10^7 colony-forming units per mL (CFU/mL). The wells were illuminated with different fluences. After illumination, a plate count method was used to determine the viable bacterial numbers (CFU/ml) in suspensions.[46] Dark controls were run in parallel. Three independent runs were carried out for each experiment. A non-coherent, white light source with interchangeable fiber bundle (model LC-122, LumaCare) was used in all photoinactivation experiments. The irradiance at the position of the samples was kept at 300 mW/cm^2, as measured by a laser power meter (Model 840011, SPER Scientific).

Characterization. The Ag@mSiO$_2$@photosensitizer hybrids were characterized by a number of techniques. A Phillips Biotwin 12 transmission electron microscope (FEI) was used to characterize the morphology. TEM samples were prepared by directly applying 10 μL of the sample in ethanol solution onto a carbon-coated copper grid (300 mesh, EMS), and allowed to dry at room temperature. Zeta potentials of the Ag@mSiO$_2$@photosensitizer hybrids were measured by a Nanotrac particle size analyzer (Microtrac). UV-Vis absorption spectra were measured using a UV-Vis spectrometer (USB4000-ISS, Ocean Optics). The loadings of photosensitizers in the Ag@mSiO$_2$@photosensitizer hybrids were determined by

measuring, *via* UV-Vis absorption spectra, the residual photosensitizers in the supernatant after centrifugation of the Ag@mSiO$_2$ nanoparticles and photosensitizer mixture to remove the Ag@mSiO$_2$@photosensitizer hybrids. The difference in the amounts between the initially added photosensitizers to the mixture and the residual photosensitizers is treated as the amount of photosensitizer loaded into the Ag@mSiO$_2$ nanoparticles, and used to calculate the loading efficiency.

Data analysis and statistics. Each experiment was performed at least in triplicate. The primary data are presented as the means with standard deviations. Differences are analyzed for statistical significance by the two-sample t-test and a p-value of < 0.05 is considered significant.

Results and discussions

Synthesis of Ag@mSiO$_2$@photosensitizer hybrids.

The design of plasmon-photosensitizer resonance coupling hybrids is inspired by the concept of supramolecular chemistry, where the building blocks are organized in such a way to exploit their interactions to the maximal extent. One active building block, AgNPs, is first prepared inside the mesoporous silica matrix, while the other active building block, photosensitizer, is subsequently adsorbed into the mesoporous silica pores. The mesopores in the silica shell can host the photosensitizers and mediate their interaction with AgNPs. They would also facilitate the diffusion of molecular oxygen and the produced singlet oxygen in and out of the silica matrix. This general platform allows us to study the singlet oxygen production from a variety of photosensitizers, including those that are hardly soluble in water. The six photosensitizers used in this study are hematoporphyrin IX dihydrochloride (HPIX), meso-porphyrin IX (PIX), meso-tetra(4-carboxyphenyl) porphine (TCPP), Cu(II) meso-tetra(4-carboxyphenyl) porphine (Cu-TCPP), tris(2,2'-bipyridyl)dichlororuthenium(II) hexahydrate (RuBPy), and rose bengal (RB).

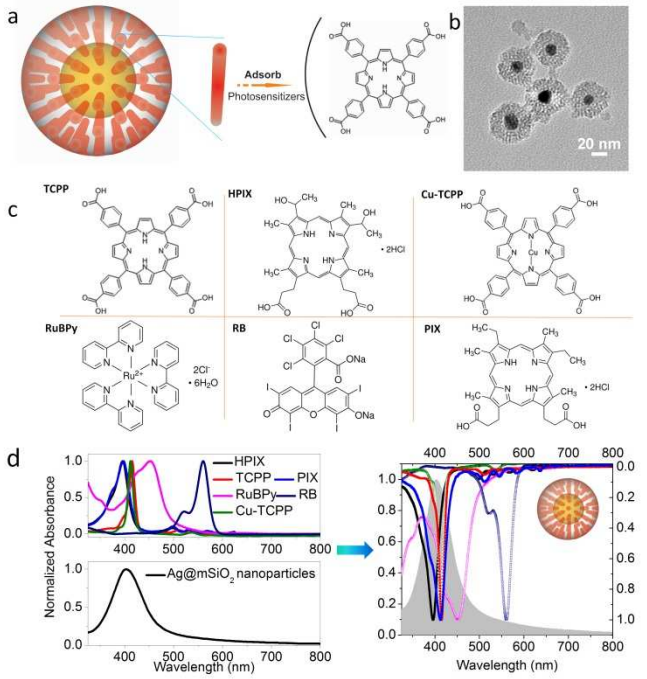

Fig. 1 (a) Schematic representation of the Ag@mSiO$_2$@photosensitizer hybrids. (b) Representative TEM image of the Ag@mSiO$_2$ nanoparticles. (c) Structures of photosensitizers used in this study. (d) Overlay of Ag@mSiO$_2$ surface plasmon and absorbance spectra of the photosensitizers.

There have been a number of reports using mesoporous silica matrix as carrier for drugs including photosensitizers.[47-49] The Ag@mSiO$_2$ core-shell nanoparticles are prepared by a simple and reproducible one-pot method, following procedures in the literature with minor modifications.[44] It combines several steps into one, including the generation and incorporation of silver nanocrystals into mesoporous silica nanoparticles, and transfer and growth of silver nanocrystals into a silver nanoparticle core inside the silica matrix. After the synthesis, different photosensitizers are directly adsorbed into the silica pores, taking advantage of the enormous porosity and surface area of the mesoporous silica nanostructures (see Fig. 1a). A typical TEM image of a spherical Ag@mSiO$_2$ nanoparticle with an average particle size of 49 nm is shown in Fig. 1b. The thickness of the mesoporous SiO$_2$ shell is ~ 17 nm and the diameter of AgNPs core ~ 15 nm. The loading efficiencies of the photosensitizers in the hybrids were determined by UV-Vis absorption. Because of the diverse molecular structures, the six photosensitizers have rather different loading efficiencies into the mesoporous silica pores under similar adsorption conditions. The measured loading efficiency of the six photosensitizers in the respective hybrids, the calculated average photosensitizer payloads (photosensitizers per nanoparticle), and the measured zeta potentials of the hybrids are summarized in Table 1. The presence of the adsorbed photosensitizers has only moderate effect on the zeta potential of the initial Ag@mSiO$_2$ core-shell nanoparticles (-26.44 mV), except for RuBPy due to its positive charge.

Table 1. Measured loading efficiency of the photosensitizers, average photosensitizer payload and zeta potential of the Ag@mSiO$_2$@photosensitizer hybrids

Ag@mSiO$_2$@photosensitizer hybrids	Loading (μg/mg)	Payload (photosensitizers/ NP)	Zeta potential (mV)
TCPP	140.7	4800	-35.46
Cu-TCPP	260.5	9600	-36.45
PIX	750	10000	-35.39
HPIX	27.4	980	-25.65
RuBPy	28.3	910	-5.80
RB	33.6	800	-31.78

Surface plasmon-photosensitizer resonance coupling.

We first study the resonance coupling between the photosensitizers and the AgNPs core in these Ag@mSiO$_2$@photosensitizer hybrids. The chemical structures of the six photosensitizers used in this study are shown in Fig. 1c. Normalized UV-Vis absorption spectra of all Ag@mSiO$_2$@photosensitizer hybrids are shown in Fig. S1. The surface plasmon peak positions in the Ag@mSiO$_2$@photosensitizer hybrids are slightly red-shifted, compared to that of the Ag@mSiO$_2$ nanoparticles at ~403 nm (Fig. S1). As shown in Fig. 1d, different photosensitizers would display different degrees of resonance coupling with AgNPs, depending on the overlap of the surface plasmon and the absorption spectra of the photosensitizers. HPIX,

TCPP, Cu-TCPP, PIX, and RuBPy have stronger resonance coupling with the AgNPs core than RB.

It is reported that plasmonic-molecular resonance coupling tends to form hybrid state(s) with new spectral characteristics.[23,50] To this end, we measure the fluorescence emission and excitation spectra of the Ag@mSiO$_2$@photosensitizer hybrids and the respective pure photosensitizer, with results shown in Fig. S2-7. In the case of TCPP, Cu-TCPP, PIX, and HPIX, all common porphyrin derivatives, the Ag@mSiO$_2$@photosensitizer hybrids display strong resonance coupling. There are significant changes in the fluorescence emission and excitation spectra of the hybrids, both in intensity and shape (Fig. S2-5, Supporting Information). The high-energy Soret band (B-band) and the low-energy quasi-allowed band (Q-band) transitions in the excitation spectra both decrease significantly. The emission bands are broadened and markedly weakened. As the concentrations of photosensitizer increase, the fluorescence intensities decrease greatly due to severe self-quenching. In contrast, Ag@mSiO$_2$@Cu-TCPP displays only slight change both in intensity and shape as compared to pure Cu-TCPP. The low fluorescence intensity of pure Cu-TCPP is probably due to the paramagnetic nature of the central copper (II).[51] In the case of RuBPy and RB (Fig. S6-7, Supporting Information), hybrids show little changes in fluorescence emission and excitation spectra, except the quenching increases with the increase of the photosensitizer concentration. The aggregation of photosensitizers in the mesoporous pores results in slight self-quenching, which is not significant compared to the quenching effect caused by the AgNP cores (Fig. S8-13). Based on the spectra of these six Ag@mSiO$_2$@photosensitizer hybrids, we consider that the hybrid state(s) formed by the surface plasmon-molecular resonance coupling affect markedly the fluorescence of the photosensitizers.

We have conducted time-resolved photoluminescence measurements of the pure photosensitizers, the mSiO$_2$@photosensitizer and the Ag@mSiO$_2$@photosensitizer hybrids (Fig. S14, and Table S1 in Supporting Information). The lifetimes of mSiO$_2$@photosensitizers are very close to those of pure photosensitizers. For the Ag@mSiO$_2$@photosensitizer hybrids, in contrast, in all cases except Cu-TCPP and RuBPy, the lifetimes of the photosensitizers are greatly reduced by the presence of the hybrid state(s), indicating the energy transfer from the excited states of photosensitizers to the AgNPs core. In the case of Cu-TCPP, the lifetime of the hybrid does not differ much from that of pure Cu-TCPP, because the lifetime of Cu-TCPP is already short due to the paramagnetic copper (II). For the Ag@mSiO$_2$@RuBPy hybrid, the effect on lifetime is insignificant.

Singlet oxygen production from the Ag@mSiO$_2$@photosensitizer hybrids.

Singlet oxygen productions from the Ag@mSiO$_2$@photosensitizer hybrids, the corresponding photosensitizers, and Ag@mSiO$_2$ nanoparticles, respectively, have been measured and calculated to determine any enhancement of singlet oxygen from the hybrids (Fig. 2 and Fig. S15-S19 in Supporting Information). The singlet oxygen enhancement factor (EF) is defined as $EF = (I_h - I_p - I_{Ag})/I_p$, where I_h, I_p, and I_{Ag} are the singlet oxygen emission intensity of the hybrids, the pure photosensitizers, and AgNPs, respectively. We notice that Ag@mSiO$_2$ nanoparticles themselves can slightly produce singlet oxygen due to the AgNP core, which is consistent with what has been reported in the literature.[10] The singlet oxygen production of Ag@mSiO$_2$ nanoparticles displays a linear relationship with regard to the concentration in the range of 0-0.6 mg/mL in water. Results summarized in Table 2 have shown that hybrids generally demonstrate significant enhancement in singlet oxygen production. With HPIX, TCPP, Cu-TCPP, PIX, and RuBPy as photosensitizer, respectively, hybrids display the enhanced production of singlet oxygen by up to three orders of magnitude, as compared to the corresponding pure photosensitizers. The only exception is Ag@mSiO$_2$@RB hybrid, most likely because of the weak resonance coupling between RB and AgNPs (Fig. S19, Supporting Information). Values of I_h and I_p are both very small when [RB] is low.

Hybrids have shown other interesting properties associated with singlet oxygen production. Four different concentrations of photosensitizers were used to investigate the relationship between the concentration and singlet oxygen production (Fig. S20, Supporting Information). We observe that singlet oxygen production increases linearly with the increased concentration of hybrids, indicating little self-quenching at higher concentrations. In contrast, for pure photosensitizers, especially TCPP and PIX of high concentrations, singlet oxygen production does not linearly increase with the increased concentrations, indicating strong self-quenching at higher concentrations. Furthermore, hybrids have displayed good stability in singlet oxygen production over long illumination time, with no decay in activity (Fig. S21, Supporting Information). We thus expect that the concentration-dependent activity and high stability of singlet oxygen production can broaden the application of these hybrids.

Table 2. Comparison of the Ag@mSiO$_2$@photosensitizer hybrids vs. pure photosensitizers in the enhancement of singlet oxygen production and fluorescence quenching.

	Enhancement of singlet oxygen production at different photosensitizer concentrations				Fluorescence quenching at different photosensitizer concentrations			
	10 μM	50 μM	100 μM	Noted in bracket	10 μM	50 μM	100 μM	Noted in bracket
TCPP	6.5	112.5	340.8	3192.5 (141 μM)	31.7	2.8	1.2	1.2 (141 μM)
Cu-TCPP	5.1	5.3	5.8	5.8 (146 μM)	1	0.3	0.4	0.6 (146 μM)
PIX	5.6	5.7	19.1	54.4 (470 μM)	17.5	9.7	2.2	0.1 (470 μM)
	1 μM	5 μM	10 μM		1 μM	5 μM	10 μM	
HPIX	8.9	6	6.8	13.3 (25 μM)	41.6	85.4	117.3	83 (25 μM)
RuBPy	7.5	6	5	4.8 (15 μM)	0.6	3	13.9	58.2 (15 μM)
RB	- -	- -	0.4	1.4 (13 μM)	2.9	18.5	47	71.5 (13 μM)

RSCPublishing

ARTICLE

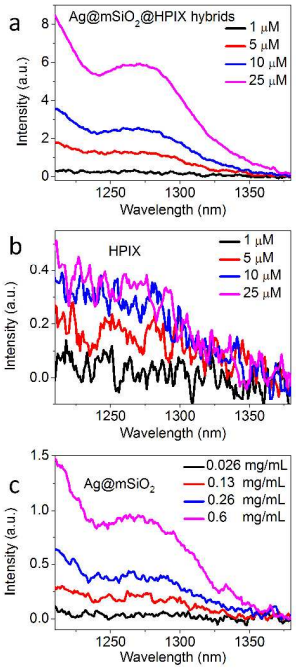

Fig. 2 Singlet oxygen luminescence spectra of (a) Ag@mSiO$_2$@HPIX hybrids, (b) HPIX, and (c) the corresponding Ag@mSiO$_2$ nanoparticles.

In the typical singlet oxygen production process (Fig. 3), photosensitizer is excited to the excited singlet state, which subsequently reaches the excited triplet state *via* intersystem crossing (ISC). When encountering ground state molecular oxygen (triplet), energy transfer takes place between the excited triplet state of the photosensitizer and molecular oxygen, leading to the generation of singlet oxygen. Experimentally, the observed singlet oxygen phosphorescence intensity I can be described as [15]

$$I = \gamma_{ex} \cdot \Phi_{ISC} \cdot P_T^{O_2} \cdot S_\Delta \cdot \Phi_p \cdot \varepsilon_{coll} \quad (1)$$

where γ_{ex} is the excitation rate, Φ_{ISC} the ISC efficiency of the photosensitizer, $P_T^{O_2}$ the fraction of the triplet photosensitizers reacted with ground state oxygen, S_Δ the efficiency of the interaction between triplet photosensitizers and ground state oxygen that results in the formation of singlet oxygen, Φ_p the phosphorescence emission quantum yield of the singlet oxygen, and ε_{coll} the light collection efficiency of the instrument.

$P_T^{O_2}$ can be further expressed as [2, 52, 53]

$$P_T^{O_2} = \frac{k_q[O_2]}{\tau^{-1} + k_q[O_2]} \quad (2)$$

where k_q is the rate constant of the triplet photosensitizer reacting with the ground state oxygen, $[O_2]$ the ground state oxygen concentration, and τ the lifetime of triplet photosensitizer in the absence of oxygen.

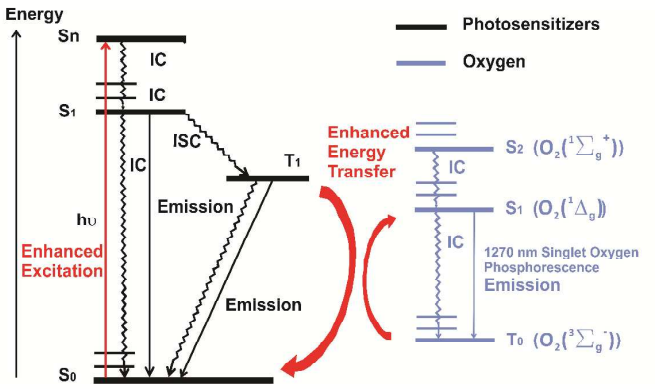

Fig. 3 Energy diagram of the photosensitized singlet oxygen production through surface plasmon-photosensitizer resonance coupling.

Investigations on metal nanoparticle enhanced ISC (Φ_{ISC}) of molecules are rather limited and usually discussed in terms of surface plasmon coupling with the excited triplet states, which can lead to metal-enhanced phosphorescence owing to the increased radiation rates.[54-56] For the Ag@mSiO$_2$@photosensitizer hybrids, the surface plasmon of the AgNP core, at ~403 nm, is far away from 1270 nm, suggesting little resonance between the surface plasmon and the single oxygen phosphorescence. It is thus expected that Φ_p remains unchanged regardless of the presence of the AgNP core. The light collection efficiency term, ε_{coll}, is system-dependent, and should be constant given all measurements are conducted under the same experimental settings. Hereby, we consider the contributions only from γ_{ex}, $P_T^{O_2}$ and S_Δ.

The enhancement in the excitation rate of photosensitizers, γ_{ex}, is possible in these Ag@mSiO$_2$@photosensitizer hybrids where the photosensitizers are adsorbed into the mesopores with close proximity to the AgNP core. The excitation of the surface plasmon resonance can greatly enhance the local electromagnetic field near the surface of the AgNPs. If there is a good spectral overlap between the surface plasmon of AgNP and the absorption of the photosensitizer, the photosensitizers will experience an enhanced excitation, resulting in the increase of γ_{ex}.[57] $P_T^{O_2}$ can be increased because excited hybrid reacts with molecular oxygen in the mesopores of silica, which increases the collision frequency, and thus rate constant, due to the small volume of the pore (mean diameter of 2.5 nm and mean length of 17 nm). Interaction between the excited triplet photosensitizer and ground state oxygen is more complex, which is essentially a triplet-triplet annihilation (TTA) process with S_Δ being the efficiency.[2,52,53,58] It has long been understood that, triplet-triplet encounter complex produce nine spin states of singlet, triplet and quintet, with statistical probability of 1/9, 3/9 and 5/9, respectively. The singlet channel is the only path leading to singlet oxygen. However, intersystem crossing among different spin states of the encounter complex is possible, which has been proposed to explain the quenching rate constant higher than 1/9 of the diffusion rate constant in the literature.[2] In that regard, the presence of AgNP could promote, through heavy atom effect, the

intersystem crossing in the triplet-triplet encounter complex, leading to a higher probability toward the singlet channel and a higher S_Δ. To sum up, it is possible that all three terms in the photosensitization process, γ_{ex}, $P_T^{O_2}$ and S_Δ, are enhanced by the presence of AgNP in the vicinity of the photosensitizers.

Photodynamic inactivation of bacteria.

The Ag@mSiO$_2$@photosensitizer hybrids demonstrate very good efficiency in broad-spectrum photodynamic inactivation of bacteria. Ag@mSiO$_2$@HPIX is used as a model system in the PDI study. We first tested Ag@mSiO$_2$@HPIX against *S. epidermidis* (ATCC 35984), a Gram-positive bacterium. Here, the bacterial culture was mixed with Ag@mSiO$_2$@HPIX hybrid in which the adsorbed HPIX concentration was 0.125-2 μM, and immediately irradiated with 40 J/cm^2 of white light. As shown in Fig. 4a-c, Fig. 5a and Fig. S22, there is a dramatic difference in the lethality against *S. epidermidis* among the hybrid, pure HPIX of same concentration, and Ag@mSiO$_2$ nanoparticles. For the hybrid, bacterial killing of ~6-log is observed when the concentration of the adsorbed HPIX in the hybrid is 2 μM. For comparison, pure HPIX and Ag@mSiO$_2$ nanoparticles display < 1-log bacterial killing under the same conditions. The enhancement in the bacterial killing efficacy can be quantified as $\log_{10}$(Enhancement killing) = $\log_{10}$(hybrid killing) - $\log_{10}$(photosensitizer killing) - $\log_{10}$(AgNPs killing). Therefore, for *S. epidermidis*, the Ag@mSiO$_2$@HPIX hybrid displays an enhancement in bacterial killing efficacy of 5-log when the concentration of the adsorbed HPIX is 2 μM. Parallel experiments conducted without light illumination show negligible antibacterial effect of the hybrid, as well as pure HPIX and Ag@mSiO$_2$ nanoparticles. While Ag ions in the Ag@mSiO$_2$ nanoparticles can be slowly released into the solution, as shown in our measurements (Fig. S23, Supporting Information), the antibacterial effect of the released Ag ions appears to be insignificant considering that there is little incubation time after the hybrid is mixed with the bacteria.[59-61] These results demonstrate the synergistic effect of Ag@mSiO$_2$@photosensitizer hybrids in the PDI against *S. epidermidis*.

We also test the antibacterial effect of the Ag@mSiO$_2$@HPIX hybrids against two Gram-negative bacteria, *E. coli* (ATCC 35218) and *A. baumannii* (ATCC 19606), the latter being a drug-resistant pathogen. Both fluence-dependence and concentration-dependence experiments were carried out to illustrate the PDI efficiency of the hybrids. As shown in Fig. 4d-i, Fig. 5b-c, and Fig. S24-S26, the killing efficacy of the Ag@mSiO$_2$@HPIX hybrid against *E. coli* and *A. baumannii* are similar to that against *S. epidermidis*. While Ag@mSiO$_2$ nanoparticles exhibit some bacterial killing under relatively high fluence, the hybrid displays a higher PDI efficiency than pure HPIX and Ag@mSiO$_2$ nanoparticles. For *E. coli*, hybrid with adsorbed HPIX concentration of 1 μM and under fluence of 400 J/cm^2 resulted in the complete eradiation of the bacterium, and an enhancement in bacterial killing of up to 4-log. In the case of *A. baumannii*, the same hybrid can completely eradiate the bacterium under fluence of 200 J/cm^2, again with an enhancement in bacterial killing of up to 4-log. We thus demonstrate that the Ag@mSiO$_2$@photosensitizer hybrids display synergistic effect in killing both Gram-positive and Gram-negative bacteria.

As a comparison, we have tested the antibacterial effect of the Ag@mSiO$_2$@RB hybrids against the three bacteria under the same fluence of illumination as in the case of Ag@mSiO$_2$@HPIX hybrids. Results are shown in the supporting information, Fig. S27-29. Ag@mSiO$_2$@RB hybrids appear to have similar photodynamic inactivation capabilities as RB itself, both displaying strong photodynamic inactivation effect against the Gram-positive *S. epidermidis* and little effect against the Gram-negative *E. coli and A. baumannii*. This is in line with what has been reported in the literature,[30] where RB is known to have limited photodynamic inactivation effect, and can only be efficient against the Gram-positive bacterium due to its cell membrane permeability. In contrast, the Ag@mSiO$_2$@HPIX hybrids are highly efficient in the photodynamic inactivation of all three bacteria, while HPIX itself has no significant photodynamic inactivation effect under the same experimental conditions.

The highly improved PDI efficiency of the Ag@mSiO$_2$@photosensitizer hybrids can be understood in the following aspects. First, the adsorbed photosensitizers in the mesopores of silica matrix result in a very high local concentration. Second, the surface plasmon-photosensitizer coupling enhances the singlet oxygen production efficiency. Third, the locally generated singlet oxygen may reach a higher concentration than when free photosensitizers act individually, causing more damage to the bacteria. In addition to their improved broad-spectrum antibacterial efficacy, we note that there are other advantages of using such Ag@mSiO$_2$@photosensitizer hybrids for PDI. These include: (1) not involving antibiotics; (2) use of non-coherent white light source; (3) no incubation required for the uptake of Ag@mSiO$_2$@photosensitizer hybrids by the bacteria; and (4) expansion to allow photosensitizers that are insoluble in water to be used in PDI applications. Therefore, we expect that the surface plasmon-photosensitizer resonance coupling hybrids can become an important platform for the development of effective and efficient photodynamic therapeutic agents against both Gram-positive and Gram-negative bacteria and possibly cancer cells.

RSCPublishing

ARTICLE

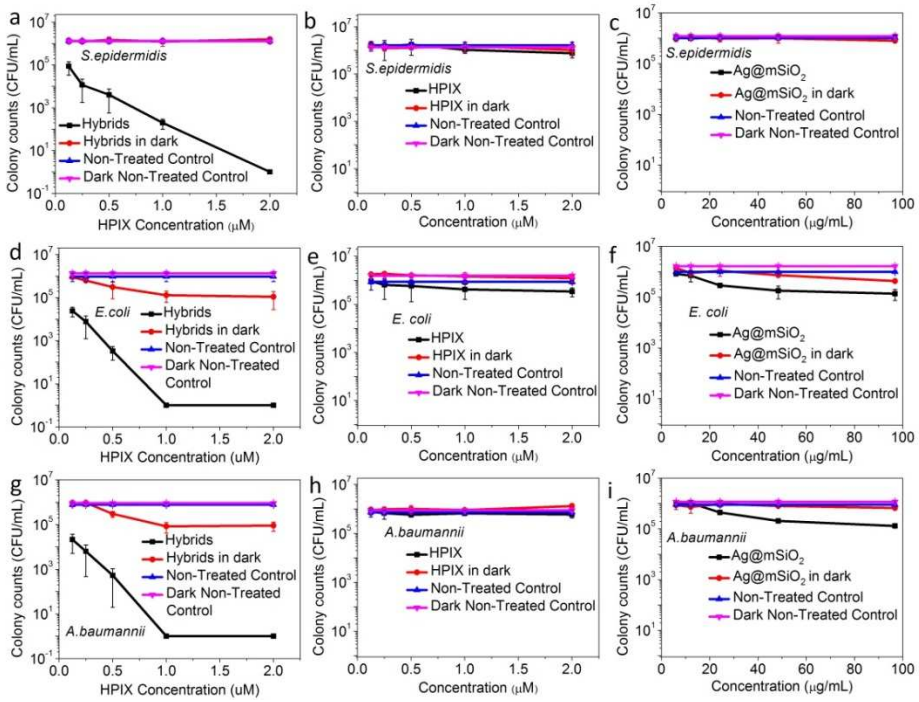

Fig. 4 Antibacterial efficacy of the Ag@mSiO$_2$@HPIX hybrid, pure HPIX and Ag@mSiO$_2$ nanoparticles on *Staphylococcus epidermidis* (ATCC 35984) (**a-d**), *Escherichia coli* (ATCC 35218) (**e-h**), and *Acinetobacter baumannii* (ATCC 19606) (**i-l**) with or without light illumination. Bacterial culture was mixed with different concentrations of photosensitizers, followed by light exposure of 40 J/cm^2 (*S. epidermidis*), 200 J/cm^2 (*A. baumannii*), or 400 J/cm^2 (*E. coli*). Results are expressed as Mean ± SD (n=3).

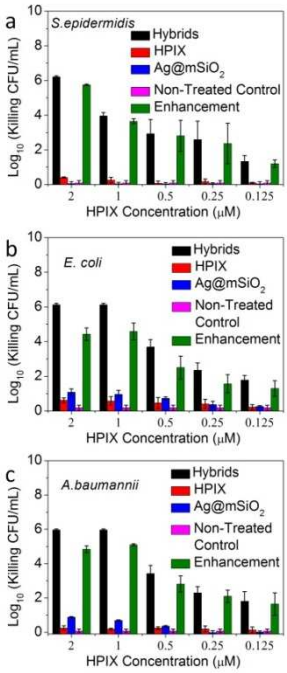

Fig. 5 Killing efficacy of Ag@mSiO$_2$@HPIX hybrid, pure HPIX and Ag@mSiO$_2$ nanoparticles on (a) *S. epidermidis* (ATCC 35984), (b) *E. coli* (ATCC 35218), and (c) *A. baumannii* (ATCC 19606) with or without light illumination, plotted as $\log_{10}$ of killing in CFU/mL vs. photosensitizer concentration.

Conclusions

In summary, we have successfully developed a general platform for singlet oxygen production based on the surface plasmon-photosensitizer resonance coupling, which significantly increases the singlet oxygen production of the photosensitizers, in some cases by up to three orders of magnitude. It is observed that the degree of the resonance coupling is directly correlated to the enhancement in singlet oxygen production. The resulting Ag@mSiO$_2$@photosensitizer hybrids demonstrate a greatly enhanced PDI efficiency against both Gram-positive and Gram-negative bacteria. The results pave way for further development of hybrid photosensitizers for photodynamic inactivation of various bacteria, including the drug-resistant pathogens.

Acknowledgements

Supports from US DOD Award DM102420 (W81XWH-11-2-0103) are gratefully acknowledged.

Notes and references

[a] Department of Chemistry, University of Cincinnati, Cincinnati, OH, United States, 45221.

[b] Drug Discovery Center, University of Cincinnati, Cincinnati, OH, United States, 45237.

* Address correspondence to Hong Tang (tangho@ucmail.uc.edu) and Peng Zhang (zhangph@ucmail.uc.edu).

Electronic Supplementary Information (ESI) available: UV-Vis absorption and fluorescence spectra, time-resolved photoluminescence transient spectra, singlet oxygen phosphorescence emission spectra, and photodynamic inactivation activities of bacteria are presented.

1. P. R. Ogilby, *Chem. Soc. Rev.*, 2010, **39**, 3181-3209.
2. N. J. Turro, V. Ramamurthy and J. C. Scaiano, *Modern Molecular Photochemistry of Organic Molecules*, University Science Books, 2010.
3. C. Schweitzer and R. Schmidt, *Chem. Rev.*, 2003, **103**, 1685-1758.
4. M. C. DeRosa and R. J. Crutchley, *Coord. Chem. Rev.*, 2002, **233–234**, 351-371.
5. R. Toftegaard, J. Arnbjerg, H. P. Cong, H. Agheli, D. S. Sutherland and P. R. Ogilby, *Pure Appl. Chem.*, 2011, **83**, 885-898.
6. D. E. J. G. J. Dolmans, D. Fukumura and R. K. Jain, *Nat. Rev. Cancer*, 2003, **3**, 380-387.
7. M. K. Kuimova, S. W. Botchway, A. W. Parker, M. Balaz, H. A. Collins, H. L. Anderson, K. Suhling and P. R. Ogilby, *Nat. Chem.*, 2009, **1**, 69-73.
8. K. Mori, M. Kawashima, M. Che and H. Yamashita, *Angew. Chem. Int. Ed.*, 2010, **49**, 8598-8601.
9. Y. Guo, S. Rogel and P. Zhang, *nanotechnology*, 2010, **21**, 065102
10. R. Vankayala, A. Sagadevan, P. Vijayaraghavan, C. L. Kuo and K. C. Hwang, *Angew.Chem. Int. Ed.*, 2011, **50**, 10640-10644.
11. R. Vankayala, C. L. Kuo, A. Sagadevan, P. H. Chen, C. S. Chiang and K. C. Hwang, *J. Mater. Chem. B*, 2013, **1**, 4379-4387.
12. X. Ragàs, A. Gallardo, Y. Zhang, W. Massad, C. D. Geddes and S. Nonell, *J. Phys. Chem. C*, 2011, **115**, 16275-16281.
13. R. Toftegaard, J. Arnbjerg, K. Daasbjerg, P. R. Ogilby, A. Dmitriev, D. S. Sutherland and L. Poulsen, *Angew. Chem. Int. Ed.*, 2008, **47**, 6025-6027.
14. Y. X. Zhang, K. Aslan, M. J. R. Previte and C. D. Geddes, *Proc. Natl. Acad. Sci. U. S. A.*, 2008, **105**, 1798-1802.
15. T. Ming, H. J. Chen, R. B. Jiang, Q. Li and J. F. Wang, *J. Phys. Chem. Lett.*, 2011, **3**, 191-202.
16. P. V. Kamat, *J. Phys. Chem. B*, 2002, **106**, 7729-7744.
17. J. R. Lakowicz, *Anal. Biochem.*, 2001, **298**, 1-24.
18. J. R. Lakowicz, *Anal. Biochem.*, 2005, **337**, 171-194.
19. R. Long, K. Mao, X. Ye, W. Yan, Y. Huang, J. Wang, Y. Fu, X. Wang, X. Wu, Y. Xie and Y. Xiong, *J. Am. Chem. Soc.*, 2013, **135**, 3200-3207.
20. M. K. Khaing Oo, Y. Yang, Y. Hu, M. Gomez, H. Du and H. Wang, *ACS Nano*, 2012, **6**, 1939-1947.
21. J. Lin, S. Wang, P. Huang, Z. Wang, S. Chen, G. Niu, W. Li, J. He, D. Cui, G. Lu, X. Chen and Z. Nie, *ACS Nano*, 2013, **7**, 5320-5329.
22. Z. Chu, C. Yin, S. Zhang, G. Lin and Q. Li, *Nanoscale*, 2013, **5**, 3406-3411.
23. H. J. Chen, T. Ming, L. Zhao, F. Wang, L. D. Sun, J. F. Wang and C. H. Yan, *Nano Today*, 2010, **5**, 494-505.
24. W. Ni, Z. Yang, H. Chen, L. Li and J. Wang, *J. Am. Chem. Soc.*, 2008, **130**, 6692-6693.
25. N. T. Fofang, T. H. Park, O. Neumann, N. A. Mirin, P. Nordlander and N. J. Halas, *Nano Lett.*, 2008, **8**, 3481-3487.
26. G. P. Wiederrecht, G. A. Wurtz and J. Hranisavljevic, *Nano Lett.*, 2004, **4**, 2121-2125.
27. G. L. Liu, Y. T. Long, Y. Choi, T. Kang and L. P. Lee, *Nat. Meth.*, 2007, **4**, 1015-1017.
28. Y. Choi, T. Kang and L. P. Lee, *Nano Lett.*, 2008, **9**, 85-90.
29. A. O. Govorov and I. Carmeli, *Nano Lett.*, 2007, **7**, 620-625.
30. M. R. Hamblin and T. Hasan, *Photochem. Photobiol. Sci.*, 2004, **3**, 436-450.
31. T. G. St. Denis, T. Dai, L. Izikson, C. Astrakas, R. R. Anderson, M. R. Hamblin and G. P. Tegos, *Virulence*, 2011, **2**, 509-520.
32. T. Maisch, *Lasers Med. Sci.*, 2007, **22**, 83-91.
33. J. P. Lyon, L. M. Moreira, P. C. G. de Moraes, F. V. dos Santos and M. A. de Resende, *Mycoses*, 2011, **54**, e265-e271.
34. G. Jori and S. B. Brown, *Photochem. Photobiol. Sci.*, 2004, **3**, 403-405.
35. M. P. Brynildsen, J. A. Winkler, C. S. Spina, I. C. MacDonald and J. J. Collins, *Nat. Biotech.*, 2013, **31**, 160-165.
36. N. S. Soukos, L. A. Ximenez-Fyvie, M. R. Hamblin, S. S. Socransky and T. Hasan, *Antimicrob. Agents Chemother.*, 1998, **42**, 2595-2601.
37. M. R. Hamblin, D. A. O'Donnell, N. Murthy, K. Rajagopalan, N. Michaud, M. E. Sherwood and T. Hasan, *J. Antimicrob. Chemother.*, 2002, **49**, 941-951.
38. S. A. G. Lambrechts, M. C. G. Aalders and J. Van Marle, *Antimicrob. Agents Chemother.*, 2005, **49**, 2026-2034.
39. T. Maisch, C. Bosl, R. M. Szeimies, N. Lehn and C. Abels, *Antimicrob. Agents Chemother.*, 2005, **49**, 1542-1552.
40. T. N. Demidova and M. R. Hamblin, *Antimicrob. Agents Chemother.*, 2005, **49**, 2329-2335.
41. E. Alves, L. Costa, C. M. B. Carvalho, J. P. C. Tome, M. A. Faustino, M. G. P. M. S. Neves, A. C. Tome, J. A. S. Cavaleiro, A. Cunha and A. Almeida, *Bmc Microbiol.*, 2009, **9**.
42. M. Ochsner, *J. Photochem. Photobiol., B*, 1997, **39**, 1-18.
43. T. A. Dahl, W. R. Midden and P. E. Hartman, *J. Bacteriol.*, 1989, **171**, 2188-2194.
44. L. Han, H. Wei, B. Tu and D. Y. Zhao, *Chem. Commun.*, 2011, **47**, 8536-8538.
45. K. Aslan, M. Wu, J. R. Lakowicz and C. D. Geddes, *J. Am. Chem. Soc.*, 2007, **129**, 1524-1525.
46. B. D. Jett, K. L. Hatter, M. M. Huycke and M. S. Gilmore, *Biotechniques*, 1997, **23**, 648-650.
47. Y. Yang, W. Song, A. Wang, P. Zhu, J. Fei and J. Li. *Phys. Chem. Chem. Phys*. 2010,**12**, 4418-4422.
48. Q. He and J. Shi. *J. Mater. Chem.* 2011, **21**, 5845-5855.
49. T. Wang, L. Zhang, Z. Su, C. Wang, Y. Liao and Q. Fu. *ACS Appl. Mater. Interfaces*. 2011, **3(7)**, 2479-2486.
50. H. Chen, L. Shao, K. C. Woo, J. Wang and H. Q. Lin, *J. Phys. Chem. C*, 2012, **116**, 14088-14095.
51. K. M. Smith, *Porphyrins and Metalloporphyrins*, Elsevier Scientific Publishing Company, 1975.
52. A. A. Abdel-Shafi, P. D. Beer, R. J. Mortimer and F. Wilkinson, *J. Phys. Chem. A*, 2000, **104**, 192-202.
53. A. A. Abdel-Shafi and F. Wilkinson, *J. Phys. Chem. A*, 2000, **104**, 5747-5757.
54. S. L. Pan and L. J. Rothberg, *J. Am. Chem. Soc.*, 2005, **127**, 6087-6094.
55. Y. X. Zhang, K. Aslan, M. J. R. Previte, S. N. Malyn and C. D. Geddes, *J. Phys. Chem. B*, 2006, **110**, 25108-25114.
56. M. J. R. Previte, K. Aslan, Y. X. Zhang and C. D. Geddes, *J. Phys. Chem. C*, 2007, **111**, 6051-6059.
57. D. Darvill, A. Centeno and F. Xie, *Phys. Chem. Chem. Phys.*, 2013, **15**, 15709-15726.
58. J. Saltiel and B. W. Atwater, in *Advances in Photochemistry*, John Wiley & Sons, Inc., 1988, vol. 14, pp. 1-90.
59. Z. m. Xiu, Q. b. Zhang, H. L. Puppala, V. L. Colvin and P. J. J. Alvarez, *Nano Lett.*, 2012, **12**, 4271-4275.
60. S. Chernousova and M. Epple, *Angew. Chem. Int. Ed.*, 2013, **52**, 1636-1653.
61. S. Eckhardt, P. S. Brunetto, J. Gagnon, M. Priebe, B. Giese and K. M. Fromm, *Chem. Rev.*, 2013, **113**, 4708-4754.

Graphic Abstract for Table of Content::

A general platform to improve singlet oxygen production via resonance coupling between surface plasmon and photosensitizers, and its broad-spectrum photodynamic inactivation of bacteria.